

Decay, interference, and chaos: How simple atoms mimic disorder

Andreas Krug¹, Sandro Wimberger^{1,2}, and Andreas Buchleitner¹

¹ Max-Planck-Institut für Physik komplexer Systeme, Nöthnitzer Str. 38, D-01187 Dresden

² Università degli Studi dell'Insubria, Via Valleggio 11, I-22100 Como

Received: May 21, 2019/ Revised version: date

Abstract. We establish a close quantitative analogy between the excitation and ionization process of highly excited one electron Rydberg states under microwave driving and charge transport across disordered 1D lattices. Our results open a new arena for Anderson localization – a disorder induced effect – in a large class of perfectly deterministic, decaying atomic systems.

PACS. 32.80.Rm Multiphoton ionization and excitation to highly excited states (e.g., Rydberg states) – 05.45.Mt Semiclassical chaos / quantum chaos – 72.15.Rn Localization effects (Anderson or weak localization)

1 Introduction

Probability transport in disordered media is an equally exciting and active field at the very heart of statistical physics. Many particle dynamics in a gas, turbulent hydrodynamic flow, the traffic flow across canonically overcrowded European highways, and, last but not least, the flow of money across stock and option markets are described by statistical means. Also in the microscopic realm we are often confronted with similar situations where it is impossible to track each single detail of the system under study – either because we ignore the precise form of the potentials which generate the dynamics, or because the number of individual constituents of the system is simply too large, or a combination of both. Well-known examples thereof are the charge transmission through mesoscopic wires, the scattering of slow neutrons off heavy nuclei, or the ion transport across cellular membranes. On this microscopic level, however, when noise is sufficiently weak, quantum interference and tunneling can dramatically affect classical probability transport, and weak [1] and strong (vulgo Anderson) localization [2], the Mott-Hubbard metal-insulator transition (see Zoller's contribution to this issue), Ericson fluctuations [3], chaos assisted tunneling [4], or (universal) conductance fluctuations [5] are just the most prominent ones of the many surprising phenomena which are born out by coherent complex transport on the microscopic scale.

On a first glance, such signatures of complex dynamics (brought about by random potentials and/or many-particle interactions) appear precisely what we do *not* expect when dealing with well isolated atomic or quantum optical systems. In the quest for an almost perfect control

of matter, we seek optimal control of the potentials which determine the dynamics (see Gerber's contribution), in time and in space. Hence, how can such low-dimensional systems mimic the complex dynamics of disordered systems? The answer is – precisely – Hamiltonian chaos, induced by nonlinear and perfectly controlled coupling of the few (at least two are needed [6]) degrees of freedom available. Given a sufficiently high density of states (in a quantum system with a discrete or quasi-discrete spectrum), such coupling can destroy the symmetries, and this is the good quantum numbers of the unperturbed dynamics, giving rise to an extremely complex spectrum characterized by an abundance of anticrossings of strongly variable size (see also Saenz' contribution) [7]. If we now prepare a wave function of arbitrary shape at an arbitrary location in phase space, its time evolution will indeed reflect the complex spectral structure, and, consequently, feature the characteristic properties of complex/disordered systems. This is the essential consequence of the random matrix conjecture [8], which states that the spectral properties of low dimensional quantum systems with underlying chaotic classical dynamics exhibit the same (universal) statistical features as complex quantum systems described by Random Matrix Theory (which took its origin in the attempt [9] to give a robust description of compound nuclear reactions – despite the little knowledge about the detailed nature of the potentials which generate the experimentally observed cross sections).

Which are the good experimental observables to monitor those features? In the usual setting of, e.g., charge transmission across a disordered lattice, transport occurs in configuration space, and the experimentalist measures a transmission probability. Such scenario can nowadays

be mimicked in quantum optical table top realizations of “ideal” lattices, where a suitable laser configuration establishes a periodic (1D or 2D or 3D) potential, with adjustable lattice constant and modulation depth. Cold atoms or ions initially prepared at one specific location can then be monitored as they move across the sample [10], and it is equally possible to enforce the transition from localized to delocalized (in configuration space) eigenstates on the lattice [11]. On the other hand, we may ask with equal right whether certain phenomena familiar from the theory of complex and/or disordered systems can be imported to electronic dynamics on the scale of a single, simple atom, with few degrees of freedom, and no *a priori* resemblance with familiar transport problems. In other words, do disorder induced phenomena have any general and robust bearing for the dynamics of simple atomic systems exposed to strong perturbations? The answer is positive, and can be elaborated for various of the above-mentioned coherent transport phenomena. For reasons of time and space, we shall specialize here to Anderson localization in driven atomic systems, and, more specifically, in atomic Rydberg states under microwave driving.

2 Anderson localization on the atomic scale

Anderson localization is a disorder induced effect, which was predicted [2] by Anderson to occur in the transmission of a charge across a one dimensional, disordered lattice. As depicted in Fig. 1, the problem cooks down to the transmission of a particle across a one dimensional random potential, at a given injection energy. The number of paths which guide the particle from the left to the right of the sample is exponentially large, since at each hump of the potential the particle can be either reflected or transmitted (with randomly distributed transmission and reflection coefficients), thus multiplying the available paths by a factor of two at each hump. The transmission amplitudes associated with these different paths acquire randomly distributed phases as they migrate through the sample, and interfere *destructively* (if the phases get homogeneously distributed over the unit circle) on exit at the right edge of the sample. Hence, a disordered potential leads to the suppression of transmission by quantum interference, and a more quantitative analysis shows that the eigenfunctions of the particle are exponentially localized over the lattice, with a characteristic localization length ξ . The final figure of merit which determines the measured conductance across the sample is ξ/L , with L the length of the sample. ξ/L determines the population of the last site right at the edge of the sample, and hence the probability flux which can escape from the sample, via the coupling matrix element connecting the last site to the leads – attached to the sample to probe the conductance.

We now import this scenario to the atomic realm, more specifically to the excitation and ionization dynamics of atomic Rydberg states under microwave driving. As mentioned above, for features of complex/disordered transport to become manifest on the atomic scale, we need

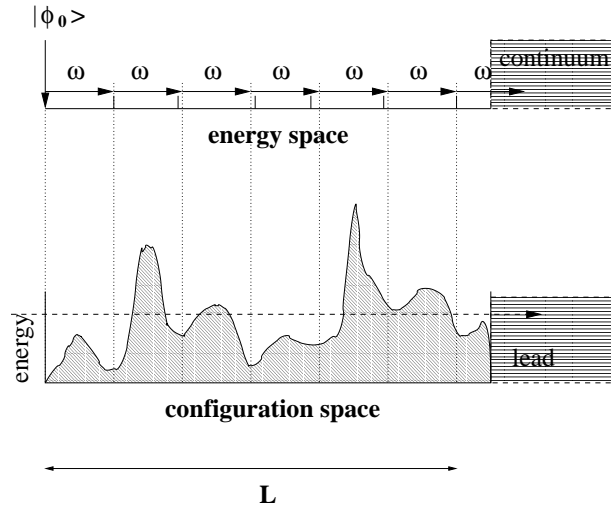


Fig. 1. The Anderson scenario: A particle (dashed horizontal line) is transmitted across a disordered potential in 1D configuration space. At each hump, the particle can be reflected or transmitted, with random reflection/transmission coefficients. The atomic ionization problem under microwave driving at frequency ω is strictly analogous if we replace reflection and transmission by emission and absorption of a photon into/from the driving field, and substitute configuration space by the energy axis. The “atomic sample length” L is then the ionization potential expressed in integer multiples of the photon energy ω , and the “sample edge” is defined by the continuum threshold. The atomic decay to the continuum (indicated by the rightmost arrow across the ionization threshold) is mediated by the one photon transition matrix element of the highest bound Rydberg state – connected to the initial state $|\phi_0\rangle$ (indicated by the vertical arrow) by a sequence of near resonant (though slightly detuned – small vertical ticks along the horizontal energy axis indicate the near resonantly coupled bound states, dashed vertical lines highlight the lattice period) one photon transitions. The population of this last bound state depends exponentially on L/ξ , with ξ the characteristic decay length of the localized wavefunction.

a high density of states actively involved in the dynamics. This is guaranteed in the Rydberg regime under microwave driving, since the typical Rydberg energy splitting lies in the microwave frequencies, and, consequently, many Rydberg states will be efficiently coupled by the drive (through subsequent, near-resonant one photon absorptions). The atomic transport process which we want to parallel with the Anderson scenario is the transport of electronic population initially prepared in a well defined atomic initial state $|\phi_0\rangle = |n_0, \ell_0, m_0\rangle$ (where spherical quantum numbers are used, as will be done throughout the sequel of this paper) towards the atomic continuum – easily measured as the ionization yield P_{ion} for given field amplitude F , field frequency ω , and interaction time t . To make the analogy complete, we have to remind ourselves of the slow variation of the level splitting with energy in the Rydberg domain. As a consequence of this unharmonicity of the spectrum, the subsequent one photon transition matrix elements which establish the “hopping matrix elements” between the different “sites” on the

energy axis mimic a random series [12], due to the imperfect matching (tantamount to quasi random detuning) of the driving frequency with the exact transition frequency (much as the simplest random number generators built on a modulo operation [13]). Consequently, if we replace “transmission/reflection” in the above transmission problem à la Anderson by “absorption/emission” in the atomic excitation process, 1D configuration space by the energy axis, and the attached leads by the atomic continuum, we encounter precisely the same scenario: An exponentially large number of paths visiting different sites (near resonantly coupled Rydberg states in the atomic problem) accumulate quasi random phases on exit from the sample, i.e., at the ionization threshold. If one photon transitions from the last near resonantly coupled bound state to the continuum define the dominant ionization channel, the atomic ionization yield will be proportional to this state’s population – determined by the localization parameter ξ/L already familiar from the Anderson scenario. Again, the sample length L is given by the number of sites which span the lattice, equivalent to the ionization potential of the atomic initial state in multiples of the driving field photon energy. Provided $\xi/L \ll 1$, the Anderson model predicts *exponential* suppression of the ionization yield due to quantum interference. Despite the strong, near resonant driving, the atom will cease absorbing energy from the field!

In fact, there already are abundant experimental data [14,15,16,18] which indicate that the above mechanism is at work in driven Rydberg states of atomic hydrogen and of alkali atoms. The central experimental result is an increase of the “scaled ionization threshold amplitude” $F_0^{(10\%)} = F^{(10\%)}n_0^4$ with increasing principal quantum number n_0 of the initial atomic state. In other words, the field amplitude $F_0^{(10\%)}$ required to ionize 10% of the atoms, at given field frequency ω and interaction time t , measured in units of the average Coulomb field $\sim n_0^{-4}$ experienced by the electron on its unperturbed initial Kepler orbit, *increases* as we *decrease* the ionization potential of the atomic initial state! This is in dramatic contradiction with the result of a classical treatment, which predicts systematically smaller ionization thresholds (due to classically chaotic phase space transport) than observed in the experiment. Consequently, there exists a range of field amplitudes which induce efficient classical ionization, whilst the experimentally observed yield is close to zero. This quantum suppression of classically chaotic ionization is interpreted as a signature of Anderson localization, and traditionally termed “dynamical localization”, such as to identify dynamical chaos as the cause of the quasi-randomization of the hopping matrix elements in the Anderson picture. However, this experimental finding is only consistent with the hypothesis of Anderson localization, it is not a clear proof – simply since one may imagine different mechanisms which inhibit the ionization process, such as semiclassical stabilization effects caused by (partial) barriers in phase space [17,19,20]. Furthermore, most experiments have been performed under slightly different experimental conditions: not only have different atomic

species been used, but also different atomic initial states were exposed to microwave fields of different frequencies ω and of variable duration t . All available experimental data exhibit large quantitative differences between the ionization threshold of atomic hydrogen on the one hand and of nonhydrogenic initial states of alkali atoms on the other, with the alkali thresholds down by a factor five to ten as compared to the hydrogen thresholds [19]. The original theory of dynamical localization in driven atomic systems [21], based on a very crude model of the actual bound state atomic dynamics, is not suited to explain these quantitative differences nor to definitively exclude processes distinct from Anderson localization which might cause the observed increase of $F_0^{(10\%)}$.

What we therefore need is an accurate theoretical treatment of microwave driven one electron Rydberg states of atomic hydrogen and of alkali atoms. Such treatment is not only required to explain the experimental findings so far available in a consistent and unified way, but also to guide future experiments which seek to test quantitative predictions which follow from Anderson localization theory for the atomic ionization process.

3 An accurate treatment of one electron Rydberg states under electromagnetic driving

Our specific problem is described by the $2\pi/\omega$ -periodic Hamiltonian

$$H(t) = \frac{\mathbf{p}^2}{2} + V_{\text{atom}}(r) + \mathbf{F} \cdot \mathbf{r} \cos \omega t, \quad r > 0, \quad (1)$$

where $V_{\text{atom}}(r)$ denotes the atomic potential seen by the valence electron, which is taken care of by a R-matrix approach [22].¹ The periodicity of H suggests to explore Floquet theory [24,25], and we therefore end up solving the Floquet eigenvalue problem

$$\mathcal{H}|\varepsilon_j\rangle = \varepsilon_j|\varepsilon_j\rangle, \quad (2)$$

with the Floquet Hamiltonian

$$\mathcal{H} = H - i\partial_t, \quad (3)$$

the spectrum of which is invariant under translations by ω . Knowledge of the $|\varepsilon_j\rangle$ and ε_j within an energy range of width ω is therefore sufficient for a complete description of the dynamics.

After a further Fourier transform of the $2\pi/\omega$ -periodic $|\varepsilon_j\rangle$, amended by complex dilation of the Hamiltonian [25,26], the eigenvalue problem is represented in a real Sturmian basis, what converts (3) into a block-tridiagonal, complex symmetric, sparse banded eigenvalue problem [22,25,27]. Note that the strong selection rules induced by the Sturmian basis are absolutely crucial for the numerical

¹ The R-matrix treatment requires input of the quantum defects of the non-hydrogenic angular momentum states of the unperturbed alkali atoms, known from high precision spectroscopy experiments [23].

treatment of our problem, since they allow for a considerable reduction of the required memory. In the parameter range typically employed in the laboratory, typical dimensions are $10^6 \times 10^4$, what nonetheless requires a very large parallel supercomputer. Indeed, all the results presented hereafter were obtained on the CRAY T3E of the High Performance Computing Center RZG of the Max-Planck-Society at Garching and, once this machine became too small, on the Hitachi SR8000-F1 of the Bavarian Academy of Sciences in Munich. Though, the availability of such a large machine is not enough. In addition, an efficient parallel implementation of the Lanczos diagonalization routine is needed, which is by no means a trivial requirement, due to considerable communication between different (and not only adjacent) processors of the parallel machine.

Once the theoretical and numerical machinery briefly sketched above is assembled, we can start our “numerical experiment”, which closely mimics the reality in the laboratory. The “counts” which the numerical experimentalist has to collect much as his colleague in the real lab are the poles of the resolvent operator in the lower half of the complex plane [28], i.e. the complex eigenvalues $\varepsilon_j = E_j - i\Gamma_j/2$ of the above eigenvalue problem. From these we can immediately extract the ionization yield [25]

$$P_{\text{ion}} = 1 - \sum_{\varepsilon} |\langle \phi_0 | \varepsilon \rangle|^2 \exp(-\Gamma_{\varepsilon} t), \quad (4)$$

for the specific choice of $|\phi_0\rangle$, t , ω , and F . Note that approx. 4000...10000 poles are typically collected here. This is simply due to the fact that the decomposition of the atomic initial state $|\phi_0\rangle$ in the dressed state basis is extremely broad in our present case [29], what is a direct consequence of the efficient destruction of good quantum numbers by the driving microwave field, and, hence, of *quantum chaos*.

4 A unified view on Anderson localization in driven atoms

With the above, we can now perform a direct comparison of the ionization thresholds of atomic Rydberg states of hydrogen and of those of alkali Rydberg states, under *precisely equivalent* conditions. For the sake of comparison to the arguably largest experimental data set (produced in the Stony Brook group [30]), we specifically choose $\omega/2\pi = 36$ GHz, $t = 327 \times 2\pi/\omega$, and $n_0 = 28 \dots 80$, $\ell_0 = m_0 = 0$, where m_0 is conserved under linearly polarized driving. Precisely as in the laboratory, we scan F from low to high values, monitor the dependence of P_{ion} on F , and extract $F_0^{(10\%)}$, for increasing values of n_0 . Fig. 2 shows a comparison of our numerical results for lithium $\ell_0 = 0$ states to laboratory results on atomic hydrogen. Surprisingly, and *in perfect contradiction* to all published experimental evidence, the nonhydrogenic (the $\ell_0 = 0$ state carries the largest quantum defect $\delta_{\ell_0=0} = 0.399468$) lithium Rydberg states exhibit essentially *the same* ionization thresholds as atomic hydrogen in regime (I), i.e.

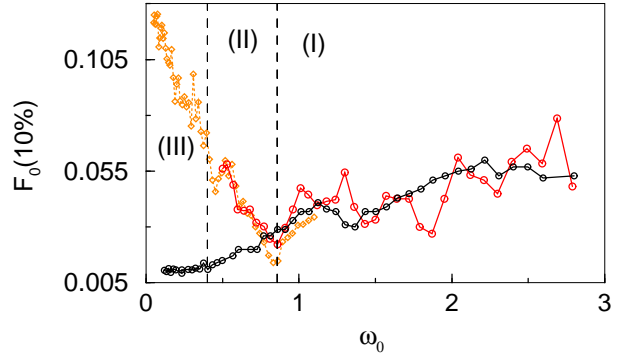


Fig. 2. Comparison of the ionization threshold of atomic hydrogen (obtained in laboratory experiments [14, 30]; light symbols) and of lithium ($\ell_0 = 0$) Rydberg states (from our numerical experiment; dark symbols) under microwave driving of duration $t = 327 \times 2\pi/\omega$ at $\omega/2\pi = 36$ GHz, in the range $n_0 = 28 \dots 80$ of principal quantum numbers (from left to right, since $\omega_0 = \omega n_0^3$). Since the laboratory values of the physical parameters are identical, the present plot in scaled units does not imply any a priori assumptions on alkali scaling laws!

for “scaled frequencies” $\omega_0 = \omega n_0^3 > 0.8$. Only for decreasing values of n_0 leading to smaller values of ω_0 do we observe an increasing discrepancy between the hydrogenic and alkali thresholds. It turns out that this can be traced back to the local density of states in the Rydberg series of the different atomic species [27]: For ω larger than the local *hydrogenic* level spacing – which scales like n_0^{-3} , hence $\omega_0 \gtrsim 1$ – the atomic excitation process is essentially unaffected by the spectral substructure in the alkalis. The atomic system offers a ladder of near resonant one photon transitions connecting $|\phi_0\rangle$ to the continuum (see Fig. 1), and it is irrelevant for the transport process whether this occurs under the participation or in the absence of non-hydrogenic states. However, once the driving frequency is smaller than the hydrogenic level spacing but still larger than the splitting between the non-hydrogenic alkali initial state and the hydrogenic manifold, the same sequence of near resonant one photon transitions can still be established in the alkali atom, whilst in hydrogen only sequences of higher order transitions are left to mediate the ionization process. Hence, the realm of the Anderson scenario outlined in the introduction extends over a wider range of principal quantum numbers in the alkali species than in atomic hydrogen, and this is indeed manifest in Fig. 2: In regime (II), with $0.4 \lesssim \omega_0 \lesssim 0.8$, the lithium data continue to exhibit decreasing thresholds with decreasing ω_0 , as an indicator of Anderson localization, whilst the hydrogenic thresholds rapidly increase as the binding potential is increased (and the local density of states is decreased, as compared to the photon energy). Finally, in regime (III), also the local energy splitting in the alkali atom is too large to be driven near resonantly by a single photon. The Anderson scenario breaks down, and the thresholds saturate in the plot of Fig. 2.

The above results hold, at least, a two-fold message: First, there is the prediction that comparable ionization thresholds for alkali and hydrogen Rydberg states will be

observed once the driving frequency is larger than the spacing between adjacent hydrogenic manifolds. This quantitative prediction can be checked immediately in state of the art laboratory experiments [18]. Second, when re-analyzing all available experimental data on the microwave ionization of non-hydrogenic alkali Rydberg states by scaling the driving field amplitude and frequency as done in Fig. 2, we find [31] that all these data were obtained in regimes (II) and (III), what explains the apparently dramatically enhanced ionization yields of non-hydrogenic alkali Rydberg states as compared to hydrogen [27, 31]. Note that this discrepancy remained a puzzle over more than one decade [30], since, so far, precisely identical experimental conditions for different atomic species were never established in the lab, and the appropriate scaling of F and ω was controversial due to the badly defined classical analog of the alkali Rydberg dynamics [16, 19, 30]. As a matter of fact, our comparison of hydrogen and lithium data in terms of scaled units in Fig. 2 do *not* imply any a priori assumptions, since they were obtained for the same laboratory values of all physical parameters, but the fact that alkali and hydrogen thresholds coincide in regime (I) *proves* that, for sufficiently high driving frequencies, the hydrogenic scaling holds even for alkalis! Even more, we do know by now [31] that also non-hydrogenic initial states of sodium and rubidium exhibit the same, hydrogenic, threshold in regime (I), what strongly suggests that this is a *universal threshold for one-electron Rydberg states*. Only this universality makes the increase of $F_0^{(10\%)}$ with ω_0 or n_0^3 a sufficient condition for the Anderson scenario to prevail, since only the universality shows that the *only* relevant ingredient is the local density of states compared to the photon energy.

There is another consequence of Anderson localization theory which can be imported to our atomic system: The localization length ξ is really well-defined a quantity only in the limit of infinite sample length, and will fluctuate around this limiting value for finite L [32]. The theoretical modelling of the conductance across an Anderson localized 1D wire of finite length L predicts a normal distribution of the logarithm of the properly normalized conductance g , if sampled over different realizations of the random lattice potential (see Fig. 1), *at fixed* ξ/L [32]. Since the (mesoscopic) conductance is given by nothing but a sum over transition matrix elements (from left to right of the sample) [33], we can come up with an analogous definition of the “atomic conductance” in our ionization problem [34],

$$g := \frac{1}{\Delta} \sum_j |\langle \phi_0 | \varepsilon_j \rangle|^2 \Gamma_j, \quad (5)$$

since the decay rates Γ_j can be understood as transition matrix elements of a suitably defined Floquet scattering problem [35] (with Δ the average level spacing). Now, if Anderson is at work in the atomic problem, the atomic conductance has to exhibit the same statistical properties as required by the theory of disordered transport – and, indeed, it does! Fig. 3 shows the distribution of the atomic conductance of a 1D model atom [34] (the electron is confined to the configuration space axis parallel to the polar-

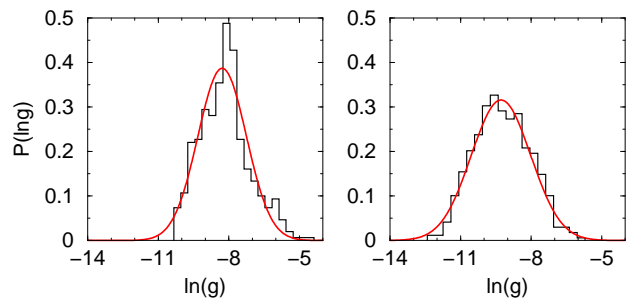


Fig. 3. Distribution (histograms) of the atomic conductance g of a 1D Rydberg atom [34, 35], sampled over 500 different realizations of the localization parameter $\xi/L = 0.2$, in the frequency range $\omega_0 = 2.0 \dots 2.5$, for $n_0 = 40$ (left) and $n_0 = 100$ (right). The lognormal fit (smooth curve) is excellent for $n_0 = 100$, in perfect quantitative agreement with Anderson localization theory [32]. The deviations from lognormal behaviour for $n_0 = 40$ reflect a finite size effect.

ization of the driving field), for fixed $\xi/L = 0.2$ (which is given in terms of n_0, F, ω , according to the original theory of dynamical localization [21]), and for two different values $n_0 = 40, 100$ of the principal quantum number.² The lognormal fit to the data is *excellent* for $n_0 = 100$, what represents another, independent and *quantitative* indicator of Anderson localization as the dominant mechanism which determines the energy exchange between the atom and the field. We also observe in Fig. 3 that the fit is significantly worse for $n_0 = 40$, what, however, does not contradict our preceding statement: At too low quantum numbers, the atomic sample size L , i.e. the number of near resonantly coupled Rydberg states between $|\phi_0\rangle$ and the continuum threshold is too small ($L \simeq 10$) to allow for a smooth exponential localization of the electronic wavefunction over the energy axis ($\xi = 0.2L = 2$). The figure therefore simply highlights a finite size effect.

Finally, Fig. 4 shows the physical imprint of the lognormal distribution of Fig. 3, the dependence of the ionization yield P_{ion} on the scaled frequency ω_0 , at $\xi/L = 0.2$ (below threshold in Fig. 2): The yield is typically very small, close to zero, but exhibits strong, erratic enhancements at particular values of ω_0 . Correspondingly, the atomic conductance g fluctuates *on a logarithmic scale*, in the right column of the figure. This is nothing but the immediate signature of the highly sensitive interference of the many paths defined by subsequent absorption and emission events mediating the transition from the initial state to the atomic continuum (see Fig. 1), and a specific signature of Anderson localization. The reader should contemplate this strongly fluctuating signal, since what fluctuates is a quantity obtained from a *weighted average* over the entire Floquet spectrum, and not just one single rate Γ_j !

² For each plot approx. 500 complex-valued spectra have been sampled, making such statistics even for the 1D model atom a rather expensive enterprise. By now, however, we have first evidence from 3D calculations that the same result can be expected for the real atom [29].

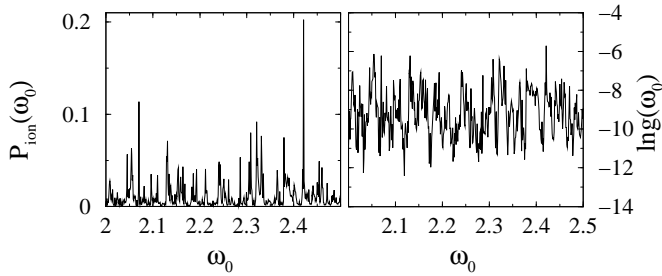


Fig. 4. Ionization yield P_{ion} (left) and atomic conductance g (right) of a 1D Rydberg atom [34,35], as a function of the scaled frequency ω_0 , in the Anderson/dynamically localized regime at $\xi/L = 0.2$, $n_0 = 100$ (below threshold in Fig. 2).

5 Conclusion

We provided two independent, quantitative proofs for Anderson localization as the dominant mechanism which governs the excitation and ionization process of strongly driven one electron Rydberg systems. Given the universal ionization threshold which we observed for atomic hydrogen and lithium Rydberg states in the high frequency parameter range, it appears legitimate to speculate that this disorder-induced quantum interference effect can be generalized for an even larger class of driven atomic or molecular system, *if only* the simple Anderson scenario can be established *on the energy axis*, as depicted in Fig. 1.

6 Acknowledgements

This paper is dedicated to Peter Lambropoulos, and might serve to illustrate a remark due to Bertrand Russell -

The pursuit of quantitative precision is as arduous as it is important.

in his “ABC of relativity”, which could be due to Peter as well.

Support as a Grand Challenge project at the Leibniz-Rechenzentrum of the Bavarian Academy of Sciences is most gratefully acknowledged.

References

1. C.A. Müller and C. Miniatura, *J. Phys.* **A35**, 10163 (2002).
2. P. Anderson, *Phys. Rev.* **109**, 1492 (1958).
3. T. Ericson, *Phys. Rev. Lett.* **5**, 430 (1960).
4. O. Bohigas, S. Tomsovic, and D. Ullmo, *Phys. Rep.* **223**, 43 (1993).
5. E. Akkermans et al. (eds.), *Mesoscopic Quantum Physics*, North Holland, Amsterdam 1995.
6. A.J. Lichtenberg and M.A. Lieberman, *Regular and Stochastic Motion*, Springer, New York 1983.
7. D. Delande and A. Buchleitner, *Adv. At. Mol. Opt. Phys.* **35**, 85 (1994).
8. O. Bohigas, M.J. Giannoni, and C. Schmidt, *Phys. Rev. Lett.* **52**, 1 (1984).
9. C.E. Porter, *Statistical theories of spectra: Fluctuations*, Academic Press, New York 1965.
10. H. Katori, S. Schlipf, and H. Walther, *Phys. Rev. Lett.* **79**, 2221 (1997).
11. M. Greiner et al., *Nature* **415**, 39 (2002).
12. N. Brenner and S. Fishman, *J. Phys.* **A29**, 7199 (1996).
13. W.H. Press et al., *Numerical Recipes in Fortran*, Cambridge University Press, Cambridge 1986.
14. E. J. Galvez, B. E. Sauer, L. Moormann, P. M. Koch, and D. Richards, *Phys. Rev. Lett.* **61**, 2011 (1988).
15. J. E. Bayfield, G. Casati, I. Guarneri, and D. W. Sokol, *Phys. Rev. Lett.* **63**, 364 (1989).
16. M. Arndt, A. Buchleitner, R. N. Mantegna, and H. Walther, *Phys. Rev. Lett.* **67**, 2435 (1991).
17. R. Graham, *Comm. At. Mol. Phys.* **25**, 219 (1991).
18. M. W. Noel, M. W. Griffith, and T. F. Gallagher, *Phys. Rev. A* **62**, 063401 (2000).
19. O. Benson, A. Buchleitner, M. Arndt, R. N. Mantegna, and H. Walther, *Phys. Rev. A* **51**, 4862 (1995).
20. A. Buchleitner, D. Delande, and J. Zakrzewski, *Phys. Rep.* **368**, 409 (2002).
21. S. Fishman, D. R. Grempel, and R. Prange, *Phys. Rev. Lett.* **49**, 509 (1982); R. Blümel and U. Smilansky, *Phys. Rev. Lett.* **52**, 137 (1984); G. Casati, B. V. Chirikov, and D. L. Shepelyansky, *Phys. Rev. Lett.* **53**, 2525 (1984).
22. A. Krug and A. Buchleitner, *Europhys. Lett* **49**, 176 (2000).
23. C.J. Lorenzen and K. Niemax, *Phys. Scr.* **27**, 300 (1983).
24. M. G. Floquet, *Annales de l'École Normale Supérieure* **12**, 47 (1883).
25. A. Buchleitner, D. Delande, and J.-C. Gay J. *Opt. Soc. Am. B* **12** (1995) 505.
26. E. Balslev and J. M. Combes, *Comm. Math. Phys.* **22**, 280 (1971).
27. A. Krug and A. Buchleitner, *Phys. Rev. Lett.* **86**, 3538 (2001).
28. A. Krug and A. Buchleitner, *Phys. Rev. A*, in press.
29. S. Wimberger, A. Krug, and A. Buchleitner, *Phys. Rev. Lett.*, in press.
30. P. M. Koch and K. A. H. Leeuwen, *Phys. Rep.* **255**, 289 (1995).
31. A. Krug, PhD thesis, Ludwig-Maximilians-Universität München, 2001, available at www.ub.uni-muenchen.de/elektronische_dissertationen/physik/Krug-Andreas.pdf.
32. J.-L. Pichard et al., *J. Phys. (Paris)* **51**, 587 (1990).
33. R. Landauer, *Philos. Mag.* **21**, 863 (1970).
34. A. Buchleitner, I. Guarneri, and J. Zakrzewski, *Europhys. Lett.* **44**, 162 (1998); S. Wimberger and A. Buchleitner, *J. Phys. A* **34**, 7181 (2001).
35. S. Wimberger, Diplomarbeit, Ludwig-Maximilians-Universität München, Munich 2000.